Vibrational overtone initiated unimolecular dissociation of $HOCH_2OOH$ and $HOCD_2OOH$: Evidence for mode selective behavior

Jamie Matthews,[1] Juliane L. Fry,[2,a)] Coleen M. Roehl,[2] Paul O. Wennberg,[2,b),c)] and Amitabha Sinha[1,b),d)]
[1]*Department of Chemistry and Biochemistry, University of California-San Diego, 9500 Gilman Drive, La Jolla, California 92093-0314, USA*
[2]*California Institute of Technology, Pasadena, California 91125, USA*

(Received 1 February 2008; accepted 27 March 2008; published online 9 May 2008)

The vibrational overtone induced unimolecular dissociation of HMHP ($HOCH_2OOH$) and HMHP-d_2 ($HOCD_2OOH$) into OH and $HOCH_2O$ ($HOCD_2O$) fragments is investigated in the region of the $4\nu_{OH}$ and $5\nu_{OH}$ bands. The unimolecular dissociation rates in the threshold region, corresponding to the $4\nu_{OH}$ band, exhibit measurable differences associated with excitation of the OH stretch of the alcohol versus the peroxide functional group, with the higher energy alcohol OH stretching state exhibiting a slower dissociation rate compared to the lower energy peroxide OH stretch in both HMHP and HMHP-d_2. Predictions using the Rice–Ramsperger–Kassel–Marcus theory give rates that are in reasonably good agreement with the measured dissociation rate for the alcohol OH stretch but considerably differ from the measured rates for the peroxide OH stretch in both isotopomers. The present results are interpreted as suggesting that the extent of intramolecular vibrational energy redistribution (IVR) is different for the two OH stretching states associated with the two functional groups in HMHP, with IVR being substantially less complete for the peroxide OH stretch. Analysis of the OH fragment product state distributions in conjunction with phase-space theory simulation gives a D_0 value of 38 ± 0.7 kcal/mole for breaking the peroxide bond in HMHP. © *2008 American Institute of Physics*. [DOI: 10.1063/1.2912063]

I. INTRODUCTION

The breaking of a chemical bond, resulting from the flow of vibrational energy within an energized molecule, represents one of the simplest of chemical transformations and is of common occurrence in many energetic environments such as combustion and atmospheric chemistry.[1–3] Much of the framework for our current understanding of these unimolecular reactions is based on a statistical approach such as that espoused by the Rice-Ramsperger-Kassel-Marcus (RRKM) theory.[4] A central hypothesis associated with this theory is that intramolecular coupling in the energized molecule is sufficiently strong so that the excitation energy, even if initially nonrandom, is statistically redistributed among all the vibrational modes of the molecule on a timescale that is fast compared to the unimolecular reaction rate. Although the vast majority of studies involving molecules excited above their reaction threshold satisfy the requirements for rapid intramolecular vibrational energy redistribution (IVR), there are examples of systems where IVR is slow or incomplete, resulting in the molecule exhibiting "nonstatistical" or mode selective behavior.[5–11] In this study, we present first results of investigating the vibrational overtone initiated unimolecular dissociation dynamics of hydroxymethyl hydroperoxide (HMHP; $HOCH_2OOH$) under low pressure room temperature conditions. The HMHP molecule is atmospherically important[12–14] and is a particularly interesting system to explore mode selectivity as it contains two OH stretching chromophores that have similar vibrational frequency, but which are located at different positions relative to the reaction center associated with the breakage of the peroxide O–O bond. Hence, one can use direct vibrational overtone excitation to excite these chromophores and investigate differences in the dissociation dynamics arising from excitation of the OH moiety directly attached to the peroxide reaction center versus the OH group situated further away, attached to the carbon end of the molecule. In this study, we present results of near threshold unimolecular dissociation rate measurements from excitation of thermal HMHP sample in the region of its third OH stretching overtone ($4\nu_{OH}$) as well as OH fragment product state distribution resulting from excitation to both the $4\nu_{OH}$ and $5\nu_{OH}$ levels (see Fig. 1). Apart from providing insight into the dissociation dynamics, the present measurements also provide data for an improved estimate of the O–O bond dissociation energy. To this end, we use the OH fragment rotational state distributions resulting from the $4\nu_{OH}$ and $5\nu_{OH}$ unimolecular dissociations in conjunction with phase space theory[15] simulations to estimate D_0 for HMHP.

Interestingly, our rate measurements in the $4\nu_{OH}$ region indicate that vibrational excitation of the lower energy peroxide OH stretch in HMHP results in a unimolecular dissociation rate that is ~40% faster than that arising from excitation of the higher frequency alcohol OH stretch, thus suggesting the presence of mode selective behavior in this

a)Present address: Department of Chemistry, University of California, Berkeley, CA 94720.
b)Authors to whom correspondence should be addressed.
c)Electronic mail: wennberg@gps.caltech.edu.
d)Electronic mail: asinha@ucsd.edu.

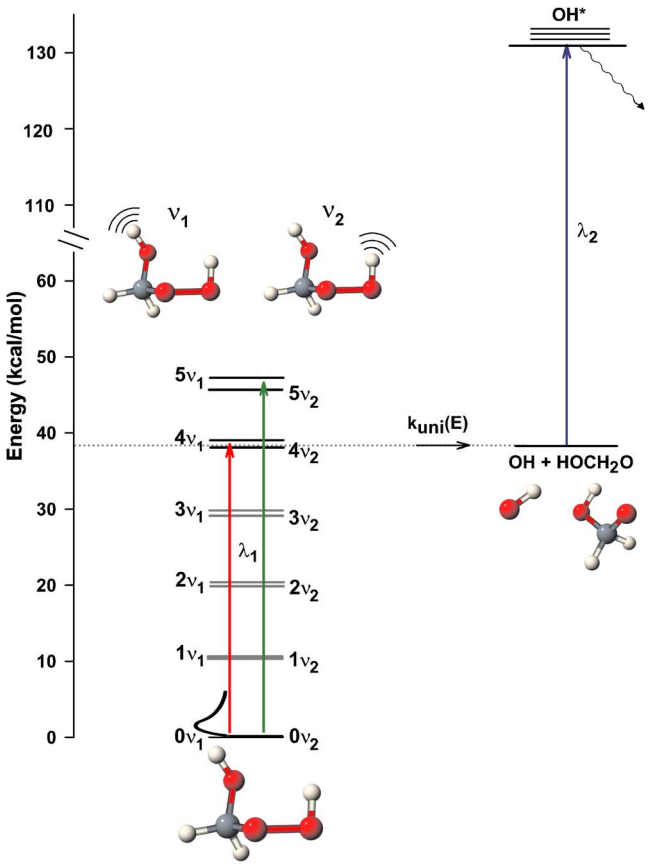

FIG. 1. (Color online) Schematic energy level diagram for vibrational overtone initiated unimolecular dissociation of HMHP. The higher frequency alcohol OH stretch is ν_1 while the peroxide OH stretch is ν_2.

molecule. This conclusion is further bolstered by our observation of a similar trend in the relative unimolecular dissociation rates from excitation of the $4\nu_{OH}$ peroxide and alcohol OH stretching chromophores in $HOCD_2OOH$ (HMHP-d_2), where the hydrogen atoms at the carbon site are replaced with deuterium. Apart from differences in the dissociation rates arising from excitation of the two *distinct* OH sites in each isotopomer, our measurements also reveal interesting variations in the dissociation rates associated with excitation of *equivalent* OH sites in the two isotopomers (HMHP versus HMHP-d_2). We find that the dissociation rate resulting from excitation of the alcohol $4\nu_{OH}$ stretching state sharply decreases, by almost a factor of 2, in going from HMHP to HMHP-d_2. By contrast, however, the dissociation rate for excitation of the peroxide $4\nu_{OH}$ state is only slightly reduced ($\sim$18%) in going to the deuterated isotopomer.

In order to interpret the above findings and compare the measured rates to the benchmark statistical behavior expected for a molecule of this size, we have also carried out RRKM calculations. Implementing these calculations involves using *ab initio* methods, available on GAUSSIAN03,[16] to first investigate the HMHP potential along the O–O bond breaking reaction coordinate in order to locate the transition state for unimolecular dissociation and then calculate the vibrational frequencies and rotational constants associated with this critical configuration. The computed *ab initio* vibrational frequencies for both the critical configuration and the reactant HMHP (HMHP-d_2) molecule are subsequently appropriately scaled and used to estimate the sum and densities of states required for implementing the RRKM theory. As we discuss below, the rate calculations provide additional support for our conclusion regarding the nonstatistical nature of the HMHP unimolecular dissociation process. Furthermore, the deviation between the calculated and measured rates appears to suggest that not only is the energy flow restricted in the energized HMHP molecule but that the extent of this restriction is different for the alcohol versus the peroxide OH stretching states in the region of the $4\nu_{OH}$ band.

II. EXPERIMENT

The experimental apparatus has been previously described and is similar to that used in our earlier study investigating unimolecular dissociation of HOCl.[9] Briefly, the photolysis chamber consists of a glass cell equipped with a viewing window for monitoring laser-induced fluorescence (LIF), two sets of mutually orthogonal side arms for introducing laser light, and several inlet ports for adding reagents. The inside of the cell is coated with halocarbon wax to minimize sample wall loss. We generate HMHP and its deuterated analog (HMHP-d_2) in a manner similar to that described in our earlier work.[17] After synthesis, the resulting liquid HMHP sample is immediately placed in a round bottom flask, situated inside a sturdy Plexiglass housing, for use during the experiments. The Plexiglass box serves as a barrier against potential peroxide explosions. The round bottom sample flask is connected through one glass valve to the photolysis chamber and through another valve to a glass bulb, directly located above it, containing $\sim$30 cm^3 of water. The valve and bulb containing water are situated outside of the Plexiglass box. After the completion of each experiment and prior to any further handling, the peroxide residue remaining in the flask, which is at reduced pressure, is quenched with water from the bulb by slowly opening the valve and filling the sample flask with water. This procedure is essential, because the residue left from the neat peroxide sample can explode when the pressure is rapidly increased to 1 atm.

We typically pump on the freshly prepared HMHP sample for several hours (8–10 h) prior to its introduction into the photolysis cell. This extended pumping minimizes contaminants such as H_2O, HCOOH, and H_2O_2 typically present in the sample as noted in our earlier study.[17] The sample pressure in the photolysis cell is maintained around 60–80 mTorr in these measurements. Laser light for excitation in the region of the third ($4\nu_{OH}$) and fourth OH stretching overtones ($5\nu_{OH}$) are generated by a dye laser (Continuum: ND60) pumped by the second harmonic of a Nd:YAG (yttrium aluminum garnet) laser (Continuum: NY82-20). The dye laser operates in the region of 600–650 nm (Rhodamine 640 + DCM mixture, 40 mJ/pulse) for the $5\nu_{OH}$ experiments and in the 720–770 nm region (LDS 750 + LDS 765 mixture, 20 mJ/pulse) for the $4\nu_{OH}$ measurements. We probe the OH photofragments resulting from unimolecular dissociation via the *A-X* transition at $\sim$308 nm using LIF. The UV probe laser radiation has a

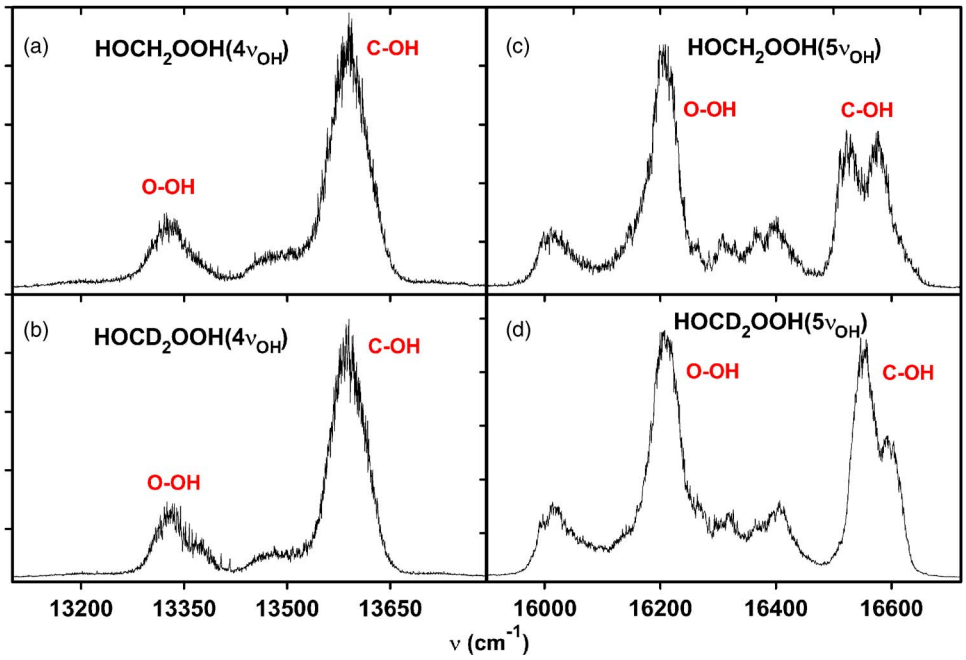

FIG. 2. (Color online) The room temperature action spectra of HMHP and HMHP-d_2 in the region of the third ($4\nu_{OH}$) and fourth ($5\nu_{OH}$) OH stretching overtones. (a) HMHP ($4\nu_{OH}$) spectrum generated by monitoring the nascent OH($N=1, {}^2\Pi_{3/2}; v=0$) rotational state. The low frequency feature appearing in the spectrum corresponds to the peroxide OH ($\sim$13 330 cm^{-1}) and the higher intensity band around $\sim$10 580 cm^{-1} corresponds to the alcohol OH. (b) HMHP-d_2 ($4\nu_{OH}$) taken under similar conditions as panel (a). (c) The fourth OH stretching overtone of HMHP($5\nu_{OH}$) generated by monitoring the nascent OH($N=3, {}^2\Pi_{3/2}; v=0$) rotational state. The peroxide OH is assigned to the band around $\sim$16 200 cm^{-1} and the alcohol OH stretch around 16 526 cm^{-1}. (d) HMHP-d_2 ($5\nu_{OH}$) taken under similar conditions as in panel (c). Fermi resonance interaction between the alcohol $5\nu_{OH}$ and $4\nu_{OH}+\nu_{CH}$ states affects the band shape (see text); reproduced from Ref. 17.

bandwidth of $\sim$0.13 cm^{-1} and is generated by frequency doubling the output of a second Nd:YAG (Continuum: NY81-20) pumped dye laser (Continuum: ND60). For the product state distribution measurements, the intensity of the probe laser is adjusted to prevent saturation of the OH transitions. The pump-probe delay is typically fixed at 20 ns for measurement of the fragment product state distribution while this delay is scanned in the unimolecular dissociation rate measurements. The OH fluorescence is collected using an $f/1$ lens system and imaged onto an end-on photomultiplier tube (PMT) (EMI 9813QB) and the signal from the PMT is subsequently sent to a gated charge integrator (LeCroy, 2249SG) and digitized for computer storage.

III. RESULTS AND DISCUSSION

A. Vibrational overtone spectra

The room temperature action spectra of HMHP and HMHP-d_2 in the vicinity of the $4\nu_{OH}$ and $5\nu_{OH}$ bands have been reported in our earlier work and are reproduced in Figs. 2(a)–2(d) for reference.[17] These spectra were generated by monitoring yields of nascent OH($v=0, {}^2\Pi_{3/2}$) fragments, respectively, in the $N=1$ and $N=3$ rotational states as the wavelength of the vibrational excitation laser is scanned over the region of the $4\nu_{OH}$ and $5\nu_{OH}$ bands. One dimensional spectral simulation using an *ab initio* dipole surface and potential along the OH stretching coordinate (CCSD(T)/aug'-cc-pVTZ) suggest that the two most prominent features appearing in the $4\nu_{OH}$ spectrum shown in Fig. 2(a) are associated with the two zeroth order OH stretching motions in the molecule, with the feature at lower frequency (13 330 cm^{-1}) corresponding to the peroxide OH stretch and the one at higher frequency (13 580 cm^{-1}) to the alcohol OH stretch.[17] As D_0 for breaking the peroxide O–O bond in HMHP is estimated to be $\sim$13 950 cm^{-1} ($\sim$39.9 kcal/mole),[17] spectral features associated with the $4\nu_{OH}$ bands lie close to the dissociation threshold. Hence, in this spectral region the observed spectral intensities are influenced not only by their absorption cross sections but also through variations in dissociation quantum yield with available energy. This is likely the main reason the peroxide OH stretching band ($\sim$13 330 cm^{-1}) is of lower intensity than the alcohol OH stretching band ($\sim$13 580 cm^{-1}) in Fig. 2(a). *Ab initio* calculations also reveal that there are three stable conformers of HMHP.[17] By including corrections for zero-point vibrational energy, the conformers are predicted to have relative energies of 0, 13, and 215 cm^{-1}. The OH stretching frequencies and anharmonicities of these conformers are very similar to one another and apparently in the $4\nu_{OH}$ region, their bands overlap to a large extent, so they are not resolved in these room temperature experiments. Also shown in Fig. 2(b) is the corresponding spectrum of $HOCD_2OOH$ (HMHP-d_2). At the resolution of the present study, the spectra of the two isotopomers nearly look identical over the region of the $4\nu_{OH}$ band.

The spectra for both HMHP and HMHP-d_2 in the $5\nu_{OH}$ spectral region are shown in Figs. 2(c) and 2(d), respectively. As in the $4\nu_{OH}$ region, there are also two primary features in the $5\nu_{OH}$ region corresponding to the two different OH stretches. Based on our earlier work, the peak at 16 205 cm^{-1} is assigned to the peroxide OH stretch while the one at 16 550 cm^{-1} is assigned to the alcohol OH group.[17] Interest-

ingly, unlike in the $4\nu_{OH}$ region, the spectra of the two isotopomers in the $5\nu_{OH}$ region exhibit noticeable differences in the vicinity of 16 550 cm^{-1} corresponding to the alcohol OH stretch. As noted in Ref. 17, Fermi resonance interaction between the zeroth-order $5\nu_{OH}$ state and the $4\nu_{OH}+\nu_{CH}$ combination band, associated with the alcohol OH stretch in HMHP, results in significant state mixing among these vibrational levels, resulting in the splitting seen in the HMHP spectrum in this region. Similar interactions have also been reported in the $5\nu_{OH}$ spectrum of methanol and formic acid.[18,19] Upon deuteration, the lower frequency of the C–D stretch removes the resonance between the $4\nu_{OH}+\nu_{CH}$ combination band and the $5\nu_{OH}$ stretching states of the alcohol moiety resulting in a single peak of higher intensity for HMHP-d_2 over the same spectral region, as shown in Fig. 2(d). Comparing the $5\nu_{OH}$ spectra of the two isotopomers in the region of the peroxide OH stretch, we see that at the present resolution, deuteration has very little visible effect on the spectral features in this region. Further analysis of the $5\nu_{OH}$ spectrum, presented in Ref. 17, suggests that the shoulder seen around 16 600 cm^{-1} in the HMHP-d_2 $5\nu_{OH}$ spectrum is likely due to the slight separation in the OH frequencies of the structural conformers at this higher overtone; this is supported by the presence of a weak, less well resolved, shoulder appearing in the corresponding HMHP peak as well.

B. Fragment product state distribution and D_0 estimate

We probe the OH fragment rotational distribution arising from unimolecular dissociation of HMHP using LIF via the diagonal transitions of the $A\ ^2\Sigma \leftarrow X\ ^2\Pi$ band. The positions of the OH spectral features are identified using the work of Dieke and Crosswhite.[20] The integrated LIF line intensities are converted to relative population using the OH Einstein B coefficients[21] and the extent of fragment alignment is assumed to be negligible in these near threshold dissociation measurements.[22] In addition to serving as a probe for differences in internal energy of the excited vibrational states undergoing unimolecular reaction, the measured OH product state distributions are used to estimate D_0 associated with breaking the O–O bond in HMHP, a parameter which we in turn utilize in the RRKM calculations. The different panels in Fig. 3 display the normalized nascent rotational distributions for the OH ($X\ ^2\Pi_{3/2}$; $v''=0$) and OH ($X\ ^2\Pi_{1/2}$; $v''=0$) spin-orbit manifolds resulting from excitation of various spectral features in the HMHP $4\nu_{OH}$ and $5\nu_{OH}$ bands. The data show that for photolysis at 13 580 cm^{-1} [Fig. 3(b)], corresponding to excitation in the $4\nu_{OH}$ region of the alcohol OH stretch, the maximum in the nascent rotational population for the lower OH ($^2\Pi_{3/2}$) spin-orbit state occurs at $N=1$ and then monotonically decrease as the OH rotational quantum number N increases. By contrast, the population in the corresponding higher energy $^2\Pi_{1/2}$ spin-orbit state, which is the less populated spin-orbit state, goes through a maximum at intermediate values of the rotational quantum number, typically $N=2$, before decreasing toward zero at higher values of N. For excitation at 13 324 cm^{-1} [see Fig. 3(a)] corresponding to the peroxide $4\nu_{OH}$ stretch, poor signal-to-noise ratio prevents us from measuring the OH($^2\Pi_{1/2}$) state populations and only the distribution associated with the lower $^2\Pi_{3/2}$ spin-orbit state is presented. It is important to point out that the feature at 13 324 cm^{-1} has a small background contribution from the HOOH impurity. Even though HOOH does not undergo unimolecular dissociation at $4\nu_{OH}$, it readily undergoes one-color two-photon vibrationally me-

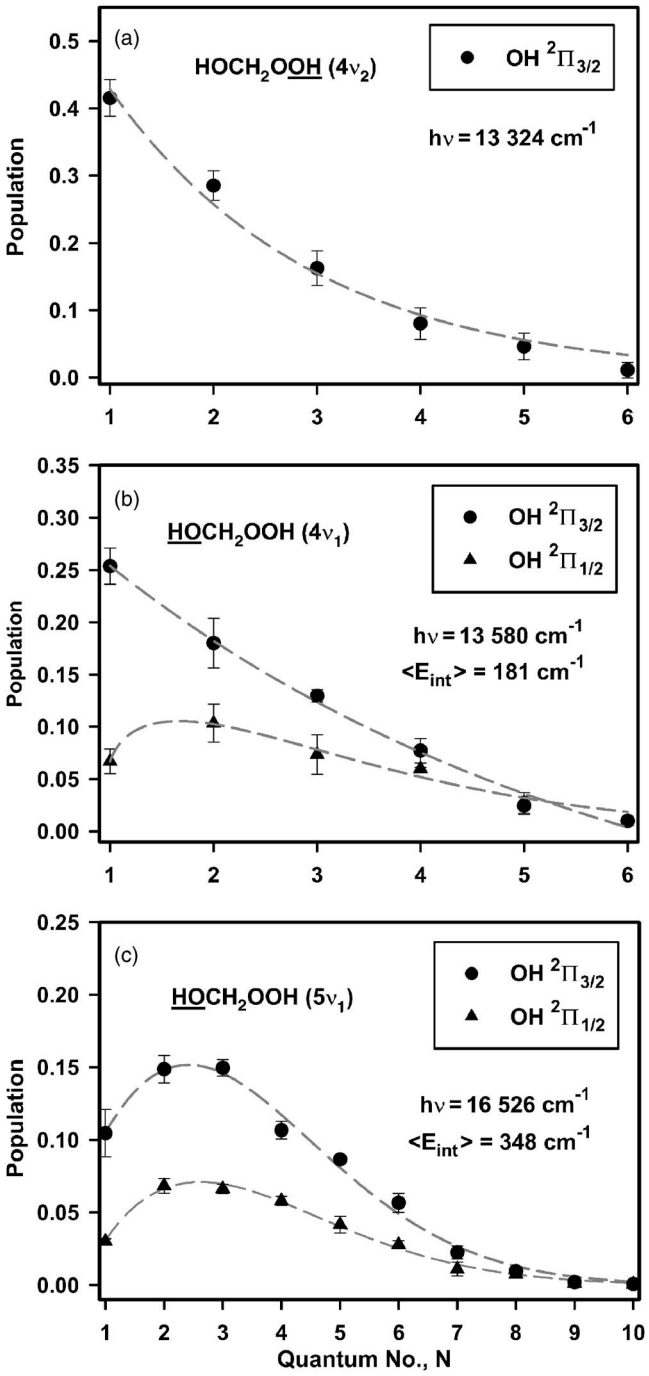

FIG. 3. Nascent rotational state distributions of the OH ($v=0, ^2\Pi_{3/2}$) and OH ($v=0, ^2\Pi_{1/2}$) states resulting from excitation of HMHP in the region of the $4\nu_{OH}$ and $5\nu_{OH}$ bands. (a) OH product state distribution resulting from excitation of the peroxide $4\nu_{OH}$ state at ~13 324 cm^{-1}. The low signal prevents probing the higher energy OH ($v=0, ^2\Pi_{1/2}$) spin-orbit state. (b) OH product state distributions resulting from excitation of alcohol $4\nu_{OH}$ state at ~13 580 cm^{-1}. (c) OH product state distributions resulting from excitation of the $5\nu_{OH}$ alcohol band at ~16 526 cm^{-1}.

TABLE I. Rotational constants and scaled [using a scaling factor of 0.9788 for harmonic frequencies from *ab initio* CCSD(T)/cc-pVDZ calculations] harmonic frequencies for reactant and products used with phase-space simulation (cm^{-1}).

	Molecule		
	HMHP	$HOCH_2O$	OH[a]
A	0.557 86	1.640 46	⋯
B	0.201 05	0.351 34	16.978[b]
C	0.167 54	0.311 94	⋯
D_J	6.07×10^{-6}	⋯	⋯
D_{JK}	-2.1×10^{-6}	⋯	⋯
D_K	2.0×10^{-6}	⋯	⋯
ν_1	3728	3815	3768
ν_2	3644	3094	⋯
ν_3	3077	2972	⋯
ν_4	2989	1415	⋯
ν_5	1459	1383	⋯
ν_6	1406	1325	⋯
ν_7	1371	1130	⋯
ν_8	1358	1094	⋯
ν_9	1249	1003	⋯
ν_{10}	1087	793	⋯
ν_{11}	1033	544	⋯
ν_{12}	1025	287	⋯
ν_{13}	805	⋯	⋯
ν_{14}	628	⋯	⋯
ν_{15}	446	⋯	⋯
ν_{16}	395	⋯	⋯
ν_{17}	334	⋯	⋯
ν_{18}	178	⋯	⋯

[a]The OH rotational lines are entered numerically in the phase-space simulations based on levels given in Ref. 20.
[b]Reference 20.

diated photodissociation in this region giving rise to highly energetic OH fragments.[23] The OH rotational distribution associated with this two-photon electronic photodissociation process, however, is well characterized[23] and the distribution arising from the unimolecular dissociation of HMHP, shown in Fig. 3(a), has this background contribution subtracted out. In contrast to the $4\nu_{OH}$ rotational state distributions, which arise from excitation near the dissociation threshold, the OH rotational distributions resulting from excitation of spectral features in the $5\nu_{OH}$ band have a qualitatively different appearance [Fig. 3(c)]. The OH $^2\Pi_{3/2}$ rotational state distributions from spectral features associated with this higher energy vibrational band exhibit a maximum peaking around $N=2$ or 3, instead of monotonically decreasing from $N=1$ as found for the band at lower excitation energy. Within our detection limits, we do not observe any measurable population in the excited vibrational state of OH from excitation of the HMHP $5\nu_{OH}$ band at 16 580 cm^{-1}.

In order to determine how well the measured OH rotational distributions are described by statistical theory, we model them using phase-space theory (PST).[15] PST makes the assumption that the transition state for near threshold unimolecular dissociation occurs at sufficiently large internuclear separation as to give a "loose" transition state, that is, a transition state where the two separating fragments are free to rotate relative to one another. The only constraints invoked

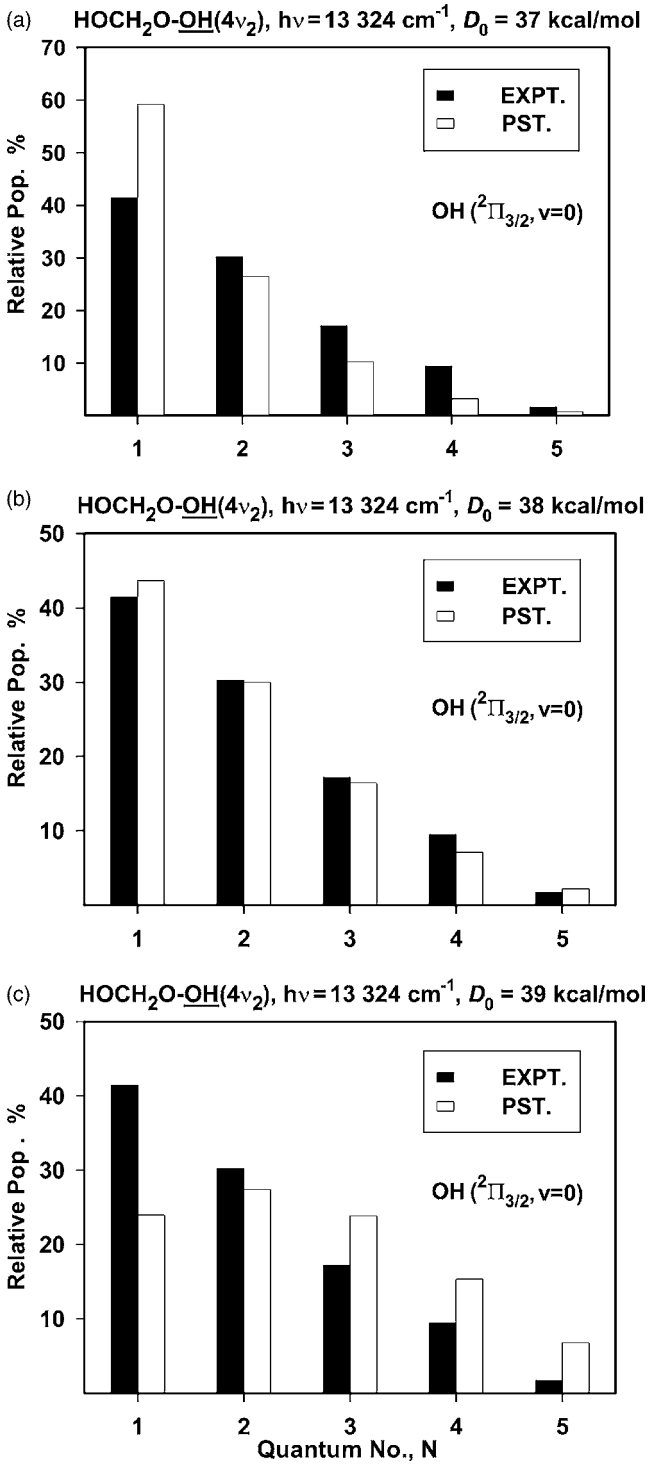

FIG. 4. Comparison of experimental and phase-space simulation of the OH ($v=0,{}^2\Pi_{3/2}$) and OH ($v=0,{}^2\Pi_{1/2}$) rotational product state distributions resulting from peroxide O–H excitation of HMHP in the region of its third OH stretching overtones ($4\nu_2$). The simulation uses excitation energy $h\nu=13\,324\ cm^{-1}$, $C_6=1.7\times10^{-58}$ erg/cm^6 and spectroscopic parameters listed in Table I. (a) Results for excitation of the peroxide $4\nu_2$ state at 13 324 cm^{-1} and $D_0=37$ kcal/mol. (b) Results for excitation of the peroxide $4\nu_2$ state at 13 324 cm^{-1} and $D_0=38$ kcal/mol. (c) Results for excitation of the peroxide $4\nu_2$ state at 13 324 cm^{-1} and $D_0=39$ kcal/mol. From these simulations we find that a value of $D_0=38\pm0.7$ kcal/mole gives the best fit to the measured HMHP OH rotational product state distributions.

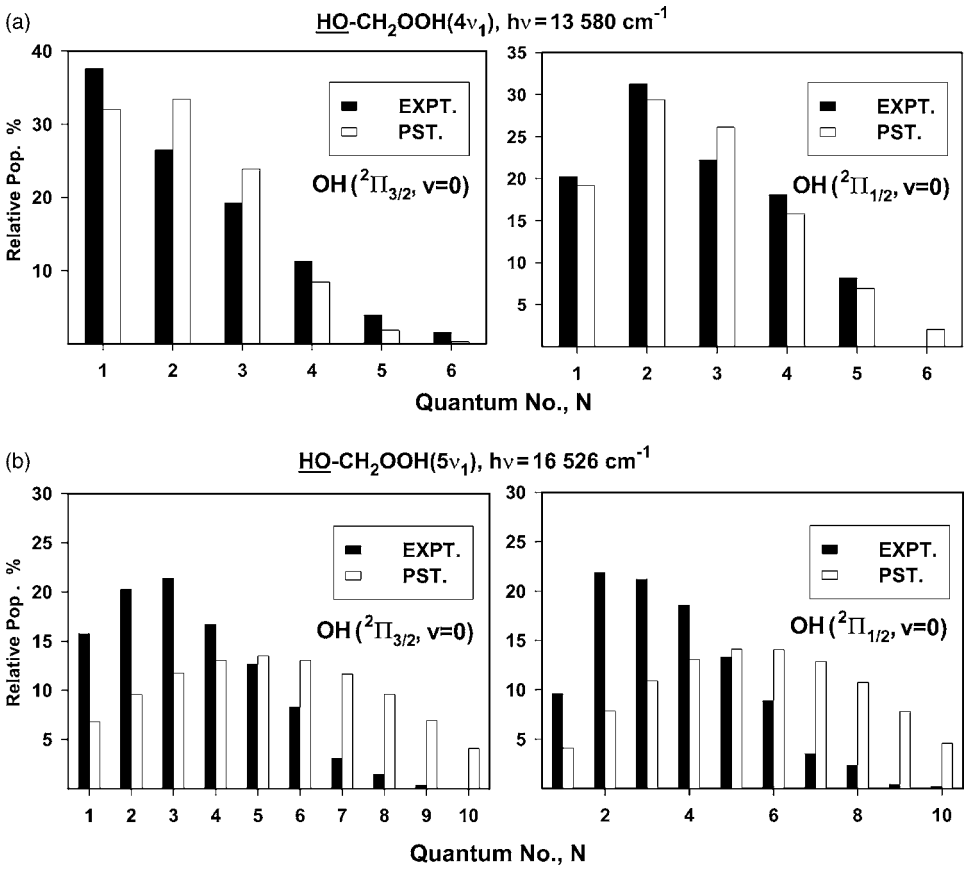

FIG. 5. Comparison of experimental and phase-space simulation of the OH ($v=0, {}^2\Pi_{3/2}$) and OH ($v=0, {}^2\Pi_{1/2}$) rotational product state distributions resulting from vibrational overtone initiated unimolecular dissociation of HMHP in the region of its third ($4\nu_1$) and fourth OH stretching overtones. The simulation uses $D_0=38$, kcal/mole $C_6=1.7\times10^{-58}$ erg/cm^6 and spectroscopic parameters listed in Table I. (a) Results for excitation of the alcohol $4\nu_1$ state at 13 580 cm^{-1}. (b) Results for excitation of the alcohol $5\nu_1$ state at 16 526 cm^{-1}.

in PST are energy and angular momentum conservation. We perform the phase-space calculations on HMHP in two steps, analogous to that described for nitric acid and HOONO.[24,25] This involves first calculating the probability that a HMHP molecule in a particular quantum state, specified by its vibrational and rotational quantum numbers, dissociates to produce OH fragments in a specified rovibrational state while conserving energy and angular momentum. We then average this probability over the distribution of HMHP states prepared by vibrational overtone excitation. The distribution of energized HMHP states prepared by the vibrational overtone excitation laser is basically assumed to be the thermal distribution of initial states, given by the Boltzmann distribution, that are then projected up to higher energy by absorption of the laser photon. We approximate $HOCH_2OOH$ ($\kappa=-0.826$) as a prolate symmetric top. The vibrational and rotational constants for both the parent and fragment molecules used in the phase-space calculations are listed in Table I. Apart from the spectroscopic parameters, the dissociation energy and long-range attraction parameter are also needed to implement the PST calculations. Using the dipole moment, polarizability, and ionization energies of the OH and $HOCH_2O$ fragments allows us to estimate the total attractive interaction parameter C_6 to be 1.7×10^{-58} erg cm^6.[26,27] We leave the dissociation energy D_0 as a fitting parameter and determine it by fitting the measured OH rotational state distributions to PST simulations using the above spectroscopic parameters and C_6 coefficient. The results of representative PST calculations associated with the peroxide $4\nu_{OH}$ band are shown in Fig. 4 for three trial D_0 values. From these simulations, represented by the unfilled bars in Fig. 4, we find that a value of $D_0=38\pm0.7$ kcal/mole gives the best fit to the measured HMHP OH rotational product state distributions arising from near threshold dissociation. This value is further confirmed by fitting the OH distributions arising from excitation of the alcohol $4\nu_{OH}$ band at 13 580 cm^{-1} using the same D_0 and C_6 values, as shown in Fig. 5(a).

Although the PST simulation fits the $4\nu_{OH}$ data reasonably well we find, however, that the fits to the $5\nu_{OH}$ band are not as good [see Fig. 5(b)]. This trend likely reflects the breakdown in the applicability of PST for states substantially above the dissociation threshold, where the critical configuration no longer corresponds to a loose transition state and vibrationally excited products can form.[28]

C. Unimolecular dissociation rate measurements

Rate measurements provide an additional probe of the unimolecular dissociation dynamics. The dissociation rates arising from excitation of various spectral features in the higher energy $5\nu_{OH}$ band are too fast to be measured with our laser system, which has a temporal resolution of ~7 ns. However, in the lower energy region of the $4\nu_{OH}$ band we find that the rates are sufficiently slow that we are able to directly measure them. Figures 6(a) and 6(b) display the results of the rate measurements associated with excitation at the peak of the primary spectral features associated, respectively, with the $4\nu_{OH}$ bands of HMHP and HMHP-d_2. In all cases the OH ($^2\Pi_{3/2}$, $N=1$, $v=0$) state is used to monitor the rates as this fragment rotational state has the largest nascent population resulting from the unimolecular dissociation in

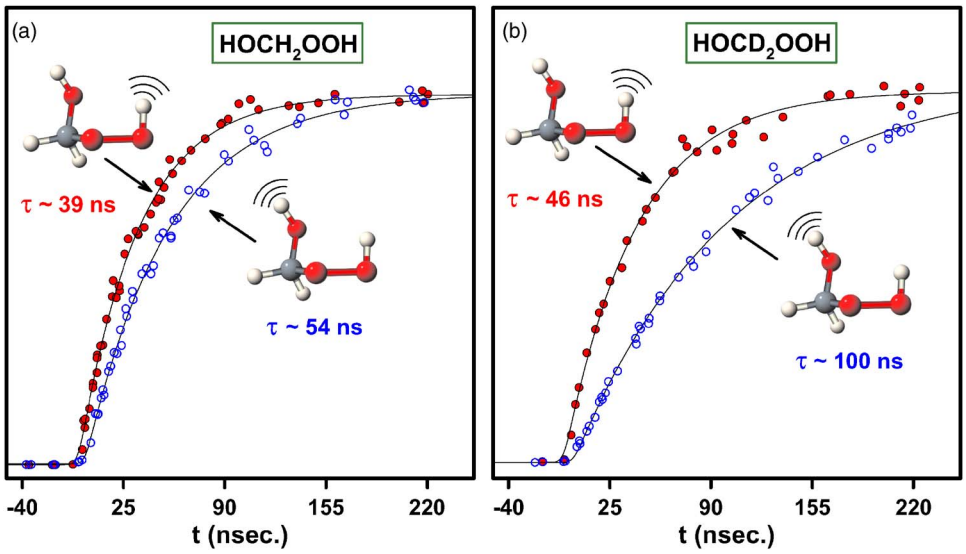

FIG. 6. (Color online) Unimolecular dissociation rate measurement resulting from excitation of the $4\nu_{OH}$ peroxide (filled circles) and alcohol (open circles) OH stretching states in HMHP and HMHP-d_2. The rates are obtained by varying the temporal delay between the overtone excitation and the probe lasers while monitoring the yield of the OH ($^2\Pi_{3/2}, N=1, v=0$) fragments. The indicated dissociation lifetimes are obtained by nonlinear least squares fitting of the data. (a) Comparison of dissociation rates resulting from excitation of the $4\nu_{OH}$ peroxide vs alcohol OH stretching states in HMHP. (b) Comparison of dissociation rates resulting from excitation of the $4\nu_{OH}$ peroxide vs alcohol OH stretching states in HMHP-d_2.

this spectral region. In the case of HMHP, Fig. 6(a) compares the rates arising from excitation at ~13 330 cm^{-1}, which corresponds to the maximum of the zeroth-order peroxide $4\nu_{OH}$ stretch versus excitation at 13 580 cm^{-1} corresponding to the peak of the zeroth-order alcohol $4\nu_{OH}$ stretching band. In addition to measuring the rates at the peak maxima, we have also measured the rates at points on either side of the main peaks, points defining the peak's full width at half maximum, and find that the variation in rates between a peak maximum and its associated shoulders to be substantially less than that between the respective peak maxima. The results are summarized in Table II. The solid lines through the data points in Figs. 6(a) and 6(b) represent a nonlinear least squares fit which includes the fragment appearance curve convoluted with the temporal profile of the vibrational excitation and probe lasers, treating the temporal profiles of both lasers as Gaussians with 7 ns full width at half maximum. Interestingly, as Fig. 6(a) shows, we find that the dissociation rate from excitation of the *lower energy* peroxide $4\nu_{OH}$ stretch of HMHP is ~40% faster than the rate associated with excitation of the higher energy alcohol $4\nu_{OH}$ stretch.

In order to see if these differences in measured rates might be due to differences in internal energies, arising from the presence of underlying vibrational hot bands, we have compared the measured OH fragment product state distributions arising from excitation of these bands.[29] We conduct this comparison because initial states having vastly different internal energies are expected to reflect this fact by exhibiting differences in their corresponding fragment product state distributions. Figure 7 compares the OH ($^2\Pi_{3/2}$) rotational state distributions arising from exciting at 13 324 cm^{-1} versus that from 13 580 cm^{-1}. Consistent with its slightly higher energy, we find that the OH rotational distribution associated with excitation at 13 580 cm^{-1} is only slightly hotter than that arising from excitation at 13 324 cm^{-1}. Thus, vastly dif-

TABLE II. HMHP dissociation rates resulting from excitation at various wavelengths in the vicinity of peroxide and alcohol $4\nu_{OH}$ bands.

Freq., ν (cm^{-1})	Lifetime (ns)	Rate (s^{-1})
	O–OH band	
13 301	40.3	24.8×10^6
13 330	39.0	25.6×10^6
13 357	42.7	23.4×10^6
	C–OH band	
13 556	50.2	19.9×10^6
13 580	53.6	18.7×10^6
13 620	46.9	21.3×10^6

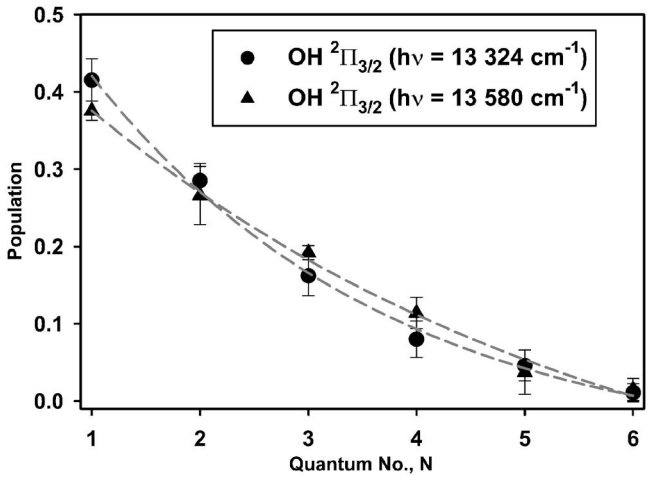

FIG. 7. Direct comparison of the measured OH ($v=0, ^2\Pi_{3/2}$) rotational product state distributions resulting from excitation of the HMHP $4\nu_2$ peroxide stretching mode at 13 324 cm^{-1} and $4\nu_1$ alcohol stretching mode at 13 580 cm^{-1}. The distributions are similar with the $4\nu_1$ alcohol stretching mode exhibiting a slightly warmer rotational temperature.

ferent initial state internal energies do not appear to be the reason for the observed differences in the dissociation rates. Indeed, the trend in internal energy, as reflected by the OH fragment rotational state distribution, is counter to that found for the measured rates since the measurements indicate that the higher energy state has the slower dissociation rate.

To further explore this apparent mode selective behavior, we have also carried out analogous rate measurements on HMHP-d_2, where the two hydrogen atoms attached to the carbon site are replaced by deuterium atoms. As Figs. 2(a) and 2(b) indicate, the vibrational bands associated with the two OH stretching chromophores in HMHP-d_2 roughly occur at the same frequency as in HMHP. Figure 6(b) shows the corresponding rate data from HMHP-d_2 resulting from excitation of its OH chromophores in the $4\nu_{OH}$ region. A comparison of Figs. 6(a) and 6(b) shows that although HMHP-d_2 follows a trend similar to that found in HMHP, with the higher energy alcohol OH stretching state giving rise to a slower dissociation rate compared to the lower energy peroxide OH stretching state, HMHP-d_2 exhibits a much larger differential between the rates for its two OH sites.

In addition to comparing dissociation rates arising from excitation of the two distinct OH sites in each isotopomer, we can also compare relative dissociation rates associated with excitation of equivalent OH sites in the two isotopomers (HMHP versus HMHP-d_2). Surprisingly, we find that deuteration at the carbon site has a large affect on the dissociation rate associated with excitation of the alcohol OH stretch, increasing its lifetime from 54 ns in HMHP to 100 ns in HMHP-d_2 while it has almost negligible affect on the lifetime associated with the peroxide OH site, where it slightly increases from 39 ns in HMHP to 46 ns in HMHP-d_2. Hence, the measured rates indicate that there is almost a factor of 2 difference in the rates between the $4\nu_{OH}$ alcohol OH stretch of HMHP versus HMHP-d_2 while for the $4\nu_{OH}$ peroxide OH stretch, the rate changes by only ~17% between the two isotopomers.

D. RRKM calculations

In order to provide a benchmark for comparison with the measured rates, RRKM calculations were carried out on both HMHP and HMHP-d_2. The D_0 value required for the RRKM calculation was obtained from the PST simulations discussed in the previous section. In applying PST, we assumed that the unimolecular dissociation occurred on a potential with negligible barrier. This assumption is reasonable as the reverse reaction involving the association of radicals, the OH and $HOCH_2O$ fragments, is expected to occur with minimal or no barrier. The issue of whether a barrier actually exists along the reaction coordinate is, however, more critical for implementation of the RRKM theory. Unlike unimolecular reactions occurring on a potential exhibiting a barrier, the simulation of reaction rates occurring on a barrierless potential is more involved and requires the application of variational RRKM theory. In order to ascertain if the HMHP potential is truly barrierless, the OPT=QST2 routine in conjunction with unconstrained optimization was used to examine the potential along the peroxide O–O bond dissociation coordinate using GAUSSIAN03.[16] The routine revealed the presence of a small ~0.9 kcal/mole barrier at an O–O bond separation distance of 2.5 Å. The transition state for HMHP unimolecular dissociation was taken to be this barrier maximum and the vibrational frequencies and rotational constants associated with this critical configuration calculated at the UCCSD(T)/cc-pVDZ level. These computed spectroscopic parameters for the transition state along with those of the reagent molecule are given in Table III. In implementing the RRKM calculations, we treated the rotational angular momentum projection quantum number, K_a, as being adiabatic.[30] Thus, this quantum number is assumed to be conserved in both the energized reactant molecule and the transition state. The rate calculation is carried out by separately considering each thermally populated reactant state characterized by the vibrational and rotational quantum numbers (v,J,K_a) and corresponding rovibrational internal energy given by $E_v+E_r(J,K_a)$. Each of these states is then promoted by the vibrational overtone excitation laser photon to generate an energized molecule with energy equal to the sum of the initial internal energy plus the photon energy. The difference between this total energy E and the barrier height E_0 gives the excess energy available for the reaction

$$E = E_v + E_r(J,K_a) + h\nu, \tag{1}$$

$$E_{\text{excess}} = E - E_0 \geqslant 0. \tag{2}$$

Only the energized states having positive excess energy are considered in the calculation. For each such state, the Boltzmann factor $P(v,J,K_a,T)$ is calculated using the expression

$$P(v,J,K_a,T) = (2J+1)\exp[-(E_v + E_r(J,K_a))/kT]. \tag{3}$$

The corresponding unimolecular rate $k(E,J,K_a)$ for each dissociating state is then calculated using the expressions

$$k(E,J,K_a) = G^{\#}[E - E_0 - E_r^{\#}(J,K_a)]/hN[E - E_r(J,K_a)]. \tag{4}$$

In the above rate expression, h is Planck's constant, $G^{\#}$ is the sum of vibrational states for the transition state at the given energy, and N is the density of vibrational states for the reactant molecule. The sum and density of states were calculated using the standard Whitten–Rabinovitch expressions using the scaled vibrational frequencies given in Table III. This procedure is repeated for each thermally populated reactant state having total energy up to 1100 cm^{-1} above the ground state. This involves considering each vibrational state falling within this energy limit, and for each such vibrational state considering values of the rotational quantum number up to $J \leqslant 80$. Furthermore, for a given J value, K_a for each state is restricted to the usual range of $(2J+1)$ values. The overall RRKM rate constant is then given by the weighted average over the Boltzmann distribution:

TABLE III. CCSD(T)/cc-pVDZ rotational constants and scaled (using scaling factor of 0.9788 for harmonic frequencies from *ab initio* calculations) harmonic frequencies used in the RRKM rates calculations for HMHP and HMHP-d_2.

	Ground state (cm^{-1})		Transition state (cm^{-1})	
	HMHP	HMHP-d_2	HMHP	HMHP-d_2
A	0.557 86	0.486 38	0.333 05	0.316 34
B	0.201 05	0.193 48	0.181 58	0.170 12
C	0.167 54	0.161 21	0.130 17	0.125 77
ν_1	3728	3727	3725	3725
ν_2	3644	3644	3595	3595
ν_3	3077	2291	3004	2217
ν_4	2989	2174	2868	2088
ν_5	1459	1368	1403	1309
ν_6	1406	1327	1353	1153
ν_7	1371	1157	1306	1019
ν_8	1358	1103	1117	958
ν_9	1249	982	1087	944
ν_{10}	1087	975	1003	844
ν_{11}	1033	942	821	673
ν_{12}	1025	871	566	559
ν_{13}	805	773	542	538
ν_{14}	628	604	466	465
ν_{15}	446	440	315	311
ν_{16}	395	373	169	167
ν_{17}	334	321	157	138
ν_{18}	178	174	⋯	⋯

$$k(T) = \sum_{v,J,Ka} P(v,J,K_a,T)k(E,J,K_a) / \sum_{v,J,Ka} P(v,J,K_a,T). \quad (5)$$

TABLE IV. RRKM rates calculated for excitation of the peroxide and alcohol $4\nu_{OH}$ stretching overtones of HMHP and HMHP-d_2.

	O–OH band		C–OH band	
D_0 (kcal/mol)	Lifetime (ns)	Rates (s^{-1})	Lifetime (ns)	Rates (s^{-1})
		HMHP		
37	35	28.6×10^6	19	52.6×10^6
37.50	63	15.9×10^6	32	31.3×10^6
37.75	87	11.5×10^6	42	23.8×10^6
37.90	105	9.52×10^6	50	20.0×10^6
38	**120**	$\mathbf{8.33\times10^6}$	**56**	$\mathbf{17.9\times10^6}$
39	259	3.86×10^6	162	6.17×10^6
40	448	2.23×10^6	361	2.77×10^6
41	725	1.38×10^6	649	1.54×10^6
Expt.	39 ± 3	$(25.6\pm2.0)\times10^6$	54 ± 4	$(18.5\pm1.4)\times10^6$
		HMHP-d_2		
37	75	13.3×10^6	39	25.6×10^6
37.50	140	7.14×10^6	68	14.7×10^6
37.75	195	5.13×10^6	91	11.0×10^6
37.90	241	4.15×10^6	109	9.18×10^6
38	**277**	$\mathbf{3.61\times10^6}$	**124**	$\mathbf{8.06\times10^6}$
39	653	1.53×10^6	382	2.62×10^6
40	1200	0.83×10^6	885	1.13×10^6
41	1973	0.51×10^6	1684	0.59×10^6
Expt.	46 ± 4	$(21.7\pm1.9)\times10^6$	100 ± 8	$(10.0\pm0.8)\times10^6$

In the above expression, the sum runs over the range of v, J, and K_a states as noted. The results of the rate calculation for $T=300$ K and several values of D_0 are given in Table IV.

Looking at the entries associated with HMHP in the upper half of Table IV, we see that for a D_0 value of 38 kcal/mole, which corresponds to our best estimate for the dissociation energy, the RRKM calculation predicts a rate that is in good agreement with the measurement for excitation of the $4\nu_{OH}$ alcohol OH stretch. However, the same calculation predicts that the rate of the corresponding peroxide OH stretch should be substantially slower and gives a value that is approximately three times lower than what is experimentally observed. The RRKM calculation for HMHP-d_2, shown in the lower half of Table IV, also exhibits similar deviations when compared to experiment. Looking at the HMHP-d_2 entries in Table IV corresponding to $D_0=38$ kcal/mole, we find that the RRKM calculations again predicts a dissociation rate for excitation of the $4\nu_{OH}$ alcohol stretch that is in reasonable accord with measurements (within ~20%). However, as before, the calculation predicts a rate for the corresponding peroxide OH stretch that is substantially slower (by a factor of 6) than what is actually experimentally observed.

IV. SUMMARY AND CONCLUSIONS

The present study, investigating the vibrational overtone induced dissociation of HMHP and HMHP-d_2, provides in-

formation about the unimolecular dissociation rates as well as an improved estimate of the molecule's bond dissociation energy. Combining the results of *ab initio* calculation, which suggests that there is a small 0.9 kcal/mole barrier to dissociation, with the measured OH fragment product state distribution and PST simulation in the region of the $4\nu_{OH}$ and $5\nu_{OH}$ bands, we estimate that D_0 is 38 ± 0.7 kcal/mole for HMHP. In coming up with this value for D_0, we note that the PST calculations are strictly valid when there are no barriers in the exit channel. Since for a given excitation energy above the dissociation threshold, the energy associated with the barrier height is expected to be unavailable for fragment internal excitation, it being primarily channeled into relative translation, the D_0 value obtained from our PST simulation is expected to provide an upper limit estimate. Given the smallness of the barrier, and the combined uncertainties associated with the PST simulations and *ab initio* calculations, the quoted ± 0.7 kcal/mole uncertainty accounts for the limitations in this approach for estimating D_0. The current value for the dissociation energy is lower than our previously estimated range (39.9–40.5 kcal/mole) which was solely based on simulation of the measured vibrational overtone spectra using estimated dissociation quantum yields.[17] A comparison of the HMHP D_0 with that of other organic peroxides shows that it is similar in value to that of t-butyl peroxide (37.6 kcal/mole)[31] but substantially lower than that of methyl hydroperoxide (42.6 kcal/mole).[32]

The dissociation rates resulting from excitation of the two distinct OH stretching chromophores in $HOCH_2OOH$ over the region of its $4\nu_{OH}$ band are found to be different, with the lower energy peroxide OH stretch exhibiting a measurable faster rate compared to the higher energy alcohol OH stretch [see Fig. 6(a)]. A measurement of the OH fragment product state distributions arising from excitation of these two bands, which provides a coarse gauge of the internal energy content associated with the corresponding vibrational overtone spectral feature, shows that the fragment rotational state distribution associated with excitation of the peroxide $4\nu_{OH}$ band at 13 324 cm^{-1} to be colder than the distribution arising from excitation of the alcohol $4\nu_{OH}$ feature at 13 580 cm^{-1}. Thus, the observed trend in dissociation rate does not appear to be a result of contribution from underlying hot bands preferentially enhancing the dissociation rate of the lower energy peroxide OH stretch. The veracity of the nonstatistical trend in dissociation rate observed in $HOCH_2OOH$ is further supported by our measurements of the corresponding rates in $HOCD_2OOH$, which also exhibits similar behavior [Fig. 6(b)]. The results of RRKM calculations, shown in Table IV, are unable to account for the observed relative rates. On an absolute scale, the RRKM calculations provide reasonable estimates for the unimolecular dissociation rates arising from excitation of the alcohol OH stretch in both HMHP and HMHP-d_2, but gives values for rates arising from the peroxide OH stretch that are substantially lower than the measurements. The observed deviation between experiment and RRKM calculation thus appears to suggest that the HMHP molecule is exhibiting nonstatistical or mode selective unimolecular dissociation.

Apart from differences in the dissociation rates associated with excitation of the two distinct OH sites in a given isotopomer, it is also interesting to compare the changes in dissociation rates associated with excitation of equivalent OH sites in HMHP versus HMHP-d_2. *Ab initio* calculations show that the replacement of the two hydrogen atoms at the carbon site with deuterium alters the frequencies of the lowest vibrational modes of the molecule only slightly. Thus the initial thermal distribution of vibrational states, which is primarily governed by the low frequency modes, is expected to be very similar in HMHP and HMHP-d_2. This is consistent with the similarity of the relative intensities appearing in the near threshold $4\nu_{OH}$ action spectra for the two isotopomers, as shown in Figs. 2(a) and 2(b). Deuterium substitution, however, does affect the relative zero-point energy associated with the reaction as well as the total density of vibrational states of the energized molecule. Based on the difference in zero-point energy between the reactant molecule and transition state, we estimate the dissociation threshold of HMHP-d_2 to be ~ 85 cm^{-1} higher in comparison to HMHP while the total density of vibrational states in the $4\nu_{OH}$ region is expected to increase from 4.05×10^5 states/cm^{-1} in HMHP to 1.16×10^6 states/cm^{-1} in HMHP-d_2. Hence, on the basis of both these factors one expects the $4\nu_{OH}$ unimolecular dissociation rates for HMHP-d_2 to be slower than those of HMHP as is indeed experimentally observed. The slower rate upon deuteration is, in fact, also reflected in the results of the RRKM calculations shown in Table IV. However, what is interesting about the present data and which the RRKM calculation is unable to reconcile, is the fact that the degree to which the rate slows down upon deuteration is experimentally found to be very different for the $4\nu_{OH}$ peroxide OH stretching state versus the alcohol OH state. We find that the dissociation rate associated with excitation of the alcohol $4\nu_{OH}$ stretching state decreases by almost a factor of 2 in going from HMHP to HMHP-d_2 while the dissociation rate for excitation of the peroxide $4\nu_{OH}$ state decreases by only $\sim 18\%$. This difference is likely not due to a secondary isotope effect, which would be expected to affect rates associated with both OH chromophores by roughly the same extent. The present findings, by contrast, apparently suggest that deuteration at the carbon site affects the coupling of the reaction coordinate to the alcohol OH moiety to a different extent than its coupling to the peroxide OH stretch.

One possible explanation for the present findings is that the OH chromophores associated with the two different functional groups, one on the methyl and the other on the peroxide moiety, exhibit different degrees of vibrational state mixing and hence different rates of IVR.[33,34] The OH attached to the methyl group, whose unimolecular dissociation rate is in fairly good agreement with the results of RRKM calculations in both HMHP and HMHP-d_2, is apparently strongly coupled to the dense manifold of "dark" background vibrational states resulting in its IVR being rather complete, which is a key requirement for the applicability of RRKM theory. By contrast, IVR is apparently more restricted in the OH chromophore associated with the peroxide functional group, thus causing its unimolecular dissociation rate to considerably differ from RRKM predictions. Numerous spectroscopic studies of IVR indicate that it typically occurs over a mul-

tiple timescale with the precise details depending on the molecule and energy range under consideration.[33,34] The initial flow of energy out of the vibrationally excited state is generally controlled by low order resonances which strongly couple the zero-order vibrational overtone excited state to a subset of background states forming a first tier of states. Additional coupling between the first-tier states and secondary tiers of background states, which themselves are not directly coupled strongly to the zero-order overtone state, redistributes the energy further among the total density of bath states over a longer timescale. Thus in an energized molecule the initial stages of IVR, which is controlled by the local density of coupled states and not the total vibrational state density, may be fast.[33–35] However, complete energy redistribution among the entire energetically accessible set of bath states, associated with the later stages of IVR, may take much longer and act as a bottleneck to energy flow.

In the present experiment, we find that, even when the total vibrational state density is increased by almost a factor of 3 through deuteration, the unimolecular dissociation rate near threshold associated with the peroxide OH stretch only slightly changes in going from HMHP to HMHP-d_2, suggesting rather minor changes in the local density of coupled states and incomplete IVR. Although relative IVR rates have not been measured for the two OH groups in HMHP and HMHP-d_2 and hence a quantitative assessment is not possible, we point out several reasons for expecting the rates to be different. First, considering HMHP: Based on the results of the $5\nu_{OH}$ spectrum, the faster initial IVR rate for the alcohol OH stretch in HMHP compared to the peroxide OH is strongly suggested by the splitting noted in the $5\nu_{OH}$ alcohol peak arising from interaction of the zero-order $5\nu_{OH}$ state and the $4\nu_{OH}+\nu_{CH}$ state. An analogous resonance is expected to be also important in the $4\nu_{OH}$ region, although its strength will likely be diminished due to the changes in energy separation of the interacting states. Second, to the extent that similar functional groups on different molecules likely exhibit comparable IVR rates, the trend for faster IVR rate for the alcohol OH compared to the peroxide OH in HMHP is supported by studies on CH_3OH and CH_3OOH.[36–38] These two molecules have OH groups that are situated in environments similar to the ones on HMHP, with methanol representing a situation where the OH is directly attached to the methyl group and methyl hydroperoxide representing the other situation where the OH group is attached to the peroxide site. These two systems differ, however, in that in the case of methyl hydroperoxide the OH is separated from the methyl rotor, which account for the bulk of the bath state density, by an intervening atom. Detailed spectroscopic measurements and theoretical analysis of the methanol $5\nu_{OH}$ and $4\nu_{OH}$ bands indicate that these OH stretching states are extensively mixed with bath states consisting of C–H stretch as well as various bending modes of the molecule.[36,37] By contrast, quasiclassical trajectory calculations carried out on vibrational overtone excited states of CH_3OOH, where the OH is located further away from the methyl rotor, indicate that this OH stretch is more isolated.[38] The calculations on methyl hydroperoxide find that the OH stretch and HOO bending modes are strongly coupled to each other but are rather isolated from the other modes in the molecule. As a consequence of this restricted IVR, the quasiclassical trajectory calculations predict CH_3OOH to exhibit mode selective behavior with respect to overtone induced unimolecular dissociation; vibrationally excited OH stretching overtone state of CH_3OOH is predicted to have a dissociation rate that is twice as fast as that of an excited C–H stretching overtone state having comparable energy.[38]

These observations, when applied to HMHP, would then suggest that the molecule is likely to exhibit vastly different IVR rates for its two OH stretching states. Although we have primarily discussed the issue of IVR for HMHP, the situation for the two OH groups in HMHP-d_2 likely also follows a similar line of reasoning. The ability of different functional groups to promote IVR to different extents has been reported in the literature with several studies noting that IVR is faster when the initially excited vibration is in close proximity to a methyl rotor or to a bond about which torsional motion occurs.[39–41] So our observation of the differences in the dissociation rate for the alcohol versus the peroxide OH stretch in HMHP and HMHP-d_2 is likely a manifestation of these effects. Further experiments on jet cooled HMHP samples, where inhomogeneous broadening can be minimized, are planned in the future to more directly probe the IVR rates of the $4\nu_{OH}$ stretching states.

ACKNOWLEDGMENTS

Funding for this work was provided by grants to A.S. from the National Science Foundation Division of Chemistry (CHE-0642640) and to P.O.W. from the National Science Foundation Division of Atmospheric Sciences (ATM-0432377). We also thank Dr. Shuping Li for assistance with certain portions of the measurements.

[1] D. J. Donaldson, G. J. Frost, K. H. Rosenlof, A. F. Tuck, and V. Vaida, Geophys. Res. Lett. **24**, 2651 (1997); D. J. Donaldson, A. F. Tuck, and V. Vaida, Chem. Rev. (Washington, D.C.) **103**, 4717 (2003).
[2] C. M. Roehl, S. A. Nizkorodov, H. Zhang, G. A. Blake, and P. O. Wennberg, J. Phys. Chem. A **106**, 3766 (2002).
[3] . J. H. Kiefer, S. Santhanam, N. K. Srinivasan, R. S. Tranter, S. J. Klippenstein, and M. A. Oehlschlaeger, Proc. Combust. Inst. **30**, 1129 (2005).
[4] P. J. Robinson and K. A. Holbrook, *Unimolecular Reactions* (Wiley, New York, 1972); W. Frost, *Theory of Unimolecular Reactions* (Academic, New York, 1973); T. Baer and W. L. Hase, *Unimolecular Reaction Dynamics* (Oxford University Press, New York, 1996); R. G. Gilbert and S. C. Smith, *Theory of Unimolecular and Recombination Reactions* (Blackwell Scientific, Oxford, 1990).
[5] T. Gilbert, T. L. Grebner, I. Fischer, and P. Chen, J. Chem. Phys. **110**, 5485 (1999).
[6] J. C. Owrutsky and A. P. Baronavski, J. Chem. Phys. **110**, 11206 (1999).
[7] S. H. Courtney, M. W. Balk, L. A. Philips, S. P. Webb, D. Yang, D. H. Levy, and G. R. Fleming, J. Chem. Phys. **89**, 6697 (1988).
[8] Y. S. Choi and C. B. Moore, J. Chem. Phys. **94**, 5414 (1991).
[9] G. Dutton, R. J. Barnes, and A. Sinha, J. Chem. Phys. **111**, 4976 (1999).
[10] M. R. Wedlock, R. Jost, and T. R. Rizzo, J. Chem. Phys. **107**, 10344 (1997).
[11] F. Reiche, B. Abel, R. D. Beck, and T. R. Rizzo, J. Chem. Phys. **116**, 10267 (2002).
[12] P. Neeb, F. Sauer, O. Horie, and G. K. Moortgat, Atmos. Environ. **31**, 1417 (1997).
[13] E. Hellpointer and S. Gab, Nature (London) **337**, 631 (1989).
[14] C. N. Hewitt and G. L. Kok, J. Atmos. Chem. **12**, 181 (1991).
[15] P. Pechukas, J. C. Light, and C. Rankin, J. Chem. Phys. **44**, 794 (1966); P. Pechukas and J. C. Light, *ibid.* **42**, 3281 (1965); J. C. Light, Faraday

Discuss. Chem. Soc. **44**, 14 (1967).
[16] M. J. Frisch, G. W. Trucks, H. B. Schlegel *et al.*, GAUSSIAN03, Revision B.04, Gaussian, Inc., Wallington, CT, 2004.
[17] J. L. Fry, J. Matthews, J. R. Lane, C. M. Roehl, A. Sinha, H. G. Kjaergaard, and P. O. Wennberg, J. Phys. Chem. A **110**, 7072 (2006).
[18] D. L. Howard and H. G. Kjaergaard, J. Chem. Phys. **121**, 136 (2004).
[19] O. V. Boyarkin, L. Lubich, R. D. F. Settle, D. S. Perry, and T. R. Rizzo, J. Chem. Phys. **107**, 8409 (1997).
[20] G. H. Dieke and H. M. Crosswhite, J. Quant. Spectrosc. Radiat. Transf. **2**, 97 (1962).
[21] W. L. Dimpfl and J. L. Kinsey, J. Quant. Spectrosc. Radiat. Transf. **21**, 223 (1979).
[22] C. H. Greene and R. N. Zare, J. Chem. Phys. **78**, 6741 (1983); Annu. Rev. Phys. Chem. **33**, 119 (1982).
[23] T. M. Ticich, M. D. Likar, H. R. Dubal, L. J. Butler, and F. F. Crim, J. Chem. Phys. **87**, 5820 (1987).
[24] A. Sinha, R. L. Vanderwal, and F. F. Crim, J. Chem. Phys. **92**, 401 (1990).
[25] J. Matthews and A. Sinha, J. Chem. Phys. **122**, 104313 (2005).
[26] We estimate the C_6 constant needed for the phase-space simulations by calculating the fragment dipole moments, ionization potentials, and polarizability at the UMP2/aug-cc-pVTZ level of theory using GAUSSIAN03 and using the appropriate equations in Ref. 27. At this level, the OH fragment has a dipole moment of 1.669 D, an ionization potential of 15.9644 eV, and polarizability of 1.00617×10^{30} m^3. The $HOCH_2O$ fragment has a dipole moment of 1.479 D, an ionization potential of 12.3627 eV, and a polarizibility of 3.58374×10^{-30} m^3
[27] I. N. Levine, *Physical Chemistry*, 4th ed. (McGraw-Hill, New York, 1995).
[28] C. Wittig, I. Nadler, H. Reisler, M. Noble, J. Catanzarite, and G. Radhakrishnan, J. Chem. Phys. **83**, 5581 (1985).
[29] We have mainly focused on comparing the OH rotational state distribution because interference from the one color two-photon vibrationally mediated photodissociation of HOOH in the region of 13 320 cm^{-1} prevented us from extracting and comparing Doppler widths associated with the unimolecular dissociation.
[30] L. Zhu, W. C. Chen, W. L. Hase, and E. W. Kaiser, J. Phys. Chem. **97**, 311 (1993).
[31] B. G. Ryu, C. R. Park, Y. Lee, S. K. Shin, and H. L. Kim, J. Photochem. Photobiol., A **149**, 15 (2002).
[32] J. Matthews, A. Sinha, and J. S. Francisco, J. Chem. Phys. **122**, 221101 (2005).
[33] D. J. Nesbitt and R. W. Field, J. Phys. Chem. **100**, 12735 (1996).
[34] K. Lehmann, G. Scoles, and B. H. Pate, Annu. Rev. Phys. Chem. **45**, 241 (1994).
[35] M. Gruebele and P. G. Wolynes, Acc. Chem. Res. **37**, 261 (2004).
[36] O. V. Boyarkin, T. R. Rizzo, and D. S. Perry, J. Chem. Phys. **110**, 11346 (1999).
[37] M. Quack and M. Willeke, J. Chem. Phys. **110**, 11958 (1999).
[38] H. Gai, D. L. Thompson, and G. A. Fisk, J. Chem. Phys. **90**, 7055 (1989).
[39] C. S. Parmenter and B. M. Stone, J. Chem. Phys. **84**, 4710 (1986).
[40] G. A. Bethardy, X. L. Wang, and D. S. Perry, Can. J. Chem. **72**, 652 (1994).
[41] D. S. Perry, G. A. Bethardy, and X. L. Wang, Ber. Bunsenges. Phys. Chem. **99**, 530 (1995).